Lab on a Chip

Standing surface acoustic wave (SSAW)-based microfluidic cytometer†

Yuchao Chen,[a] Ahmad Ahsan Nawaz,[a] Yanhui Zhao,[a] Po-Hsun Huang,[a] J. Phillip McCoy,[b] Stewart J. Levine,[b] Lin Wang[c] and Tony Jun Huang*[a]

The development of microfluidic chip-based cytometers has become an important area due to their advantages of compact size and low cost. Herein, we demonstrate a sheathless microfluidic cytometer which integrates a standing surface acoustic wave (SSAW)-based microdevice capable of 3D particle/cell focusing with a laser-induced fluorescence (LIF) detection system. Using SSAW, our microfluidic cytometer was able to continuously focus microparticles/cells at the pressure node inside a microchannel. Flow cytometry was successfully demonstrated using this system with a coefficient of variation (CV) of less than 10% at a throughput of ~1000 events s^{-1} when calibration beads were used. We also demonstrated that fluorescently labeled human promyelocytic leukemia cells (HL-60) could be effectively focused and detected with our SSAW-based system. This SSAW-based microfluidic cytometer did not require any sheath flows or complex structures, and it allowed for simple operation over a wide range of sample flow rates. Moreover, with the gentle, bio-compatible nature of low-power surface acoustic waves, this technique is expected to be able to preserve the integrity of cells and other bioparticles.

Introduction

Flow cytometry is a gold standard for cell screening and analysis.[1,2] To date, it is one of the most efficient and effective approaches to analyze a large sample population with single cell resolution. However, several drawbacks limit the use of conventional flow cytometers in many applications, such as for point-of-care diagnostics, as well as limiting its popularity outside of centralized facilities.[3–5] These practical limitations include its bulky size, high maintenance costs, and the need for a skilled operator. In the past decade, the application of microfluidic technologies[6–16] toward improving the design of flow cytometers has shown great potential to overcome these limitations. By integrating tiny and cost-effective microfluidic devices with modules for optical detection and data acquisition, it is possible to realize portable, inexpensive, low-maintenance (disposable), and user-friendly (semi-automated) microfluidic cytometers.

One of the core features of a flow cytometer is the ability to focus a stream of particles or cells into a single-file line. This allows particles or cells to travel past an illumination spot one at a time with nearly identical velocities for consistent optical measurement. Leveraging microfluidics,[17–20] a variety of techniques have been developed to focus particles or cells.[21] One simple method employed two outer sheath flows in parallel to sandwich and compress a central sample flow for two-dimensional (2D) focusing.[22–25] However, without confinement in the vertical direction, particles in the sample flow have a non-uniform velocity distribution, resulting in less precise measurements. Three-dimensional (3D) hydrodynamic focusing techniques have been developed with the introduction of additional sheath flows from the vertical direction or the generation of "microfluidic drifting" by horizontal sheath flows.[26–41] Although 3D-focused particles can be more precisely measured, some problems still remain with these hydrodynamic focusing techniques. First of all, most of the 3D hydrodynamic focusing techniques require several sheath flows with much higher flow rates compared to the sample flow. This means an increase in the number of pumps, a high consumption of fluids, and a larger volume of potentially hazardous waste to store and process, which are all barriers to the miniaturization of a flow cytometer system. Moreover, in order to deliver sheath flows from the vertical direction, multi-layer 3D-structures are usually necessary to realize these microfluidic devices, increasing the complexity and difficulty in the device fabrication and operation. Finally, for some 3D hydrodynamic focusing techniques, each fluid flow rate has to be precisely controlled; otherwise, 3D focusing cannot be ideally achieved. This places strict requirements on the performance

[a] *Department of Engineering Science and Mechanics, The Pennsylvania State University, University Park, PA, 16802, USA. E-mail: junhuang@psu.edu*
[b] *National Heart, Lung, and Blood Institute (NHLBI), Bethesda, MD, 20810, USA*
[c] *Ascent Bio-Nano Technologies Inc., State College, PA, 16801, USA*

† Electronic supplementary information (ESI) available: Including a video of SSAW focusing. See DOI: 10.1039/c3lc51139a

of the pumps. Sheathless 3D hydrodynamic focusing can also be achieved using inertial microfluidics.[42–45] This technique circumvents some of the problems associated with conventional hydrodynamic focusing techniques, although it requires long channels and has to operate at very high flow rates, which may not be ideal in certain circumstances.

Besides hydrodynamic focusing, some other particle-focusing techniques have been demonstrated, using approaches such as dielectrophoresis (DEP) forces, electrokinetics, and acoustics.[46–49] Among these approaches, acoustic-based microparticle manipulation techniques appear to be ideal because they are sheathless, non-invasive, and applicable to virtually all microparticles.[41,50–62] Recently our group has demonstrated that standing surface acoustic waves (SSAW) can be used to achieve 3D focusing of microparticles without using sheath fluid.[63,64] In this work, we take advantage of the SSAW-assisted 3D focusing and demonstrate a high-performance, sheathless microfluidic cytometer by integrating the SSAW-based 3D focusing microdevice with a laser-induced fluorescence (LIF) detection system. In our study, this flow cytometer was characterized with calibration beads and then was successfully used to identify two groups of microparticles with different diameters. Cellular samples were also used to establish the performance of the SSAW-based flow cytometry system. Compared to the existing microfluidic cytometers, our SSAW-based flow cytometer achieves sheathless, high-resolution particle/cell focusing and detection without requiring any complex device structures. This design performs well over a wide range of sample flow rates, which enables excellent flexibility and simple integration into an automated, portable microfluidic cytometer. In addition, the power intensity and frequency used in the SSAW-based particle/cell focusing technique is in a similar range as those used in ultrasonic imaging, which has been widely used in various stages of pregnancy and proven to be extremely safe over the past half a century. This implies that our SSAW-based microfluidic cytometry could be potentially bio-compatible to cells and other biological samples.

Materials and methods

Device fabrication

A lithium niobate (LiNbO$_3$) wafer (Y+128° X-propagation, Red Optronics, USA) was used as a piezoelectric substrate to generate the SSAW. The two sets of interdigitated transducers (IDTs) on the substrate were simultaneously patterned using a photolithography process.[65–67] First, photoresist was spin-coated on the wafer and patterned. Next, two thin-film metal layers (Cr/Au, 50 Å/500 Å) were sequentially deposited with an e-beam evaporator (Semicore Corp, USA). Two arrays of electrodes, which formed each IDT, were fabricated on the LiNbO$_3$ substrate by a lift-off process. The two sets of IDTs, positioned on either side of a PDMS microchannel, were designed to each have 20 pairs of electrodes with uniform electrode widths and spacing gaps (both 50 μm). Both IDTs could generate identical surface acoustic waves (SAWs)

with a wavelength of 200 μm at a resonance frequency of 19 MHz. AC signals, generated by a RF signal generator (E4422B, Agilent, USA) and amplified with a power amplifier (100A250A, Amplifier Research, USA), were applied to both IDTs to generate two travelling SAWs along the delay line and formed a one-dimensional (1D) SSAW field. In our experiments, we used 37.5 mW as the input power for SSAW generation. A single-layer PDMS microchannel (100 μm in width, 60 μm in height, and 10 mm in length) was fabricated by standard soft lithography and the mold-replica technique. After aligning and bonding the PDMS onto the LiNbO$_3$ substrate, the microchannel was positioned between the two IDTs with a single pressure node located along the centerline long axis of the microchannel.

Experimental setup

The assembled SSAW-based, 3D-focusing microdevice was mounted onto the mechanical stage of an inverted microscope (TE2000U, Nikon, Japan). A high-speed camera (SA4, Photron, Japan) and a CCD camera (CoolSNAP HQ2, Photometrics, USA) were used to record the particle/cell-focusing process and fluorescent images. For side-view imaging, a prism (2.0 mm, Tower Optical, USA) was used to refract both fluorescent excitation signals and emission signals. A syringe pump (neMESYS, Cetoni GmbH, Germany) was used to inject the samples into the microchannel and to control the flow rate at 15 μL min^{-1} for microparticles and 10 μL min^{-1} for the cell sample. The LIF detection system is illustrated in Fig. 1. A laser illuminator (488 nm FiberTEC^{II}, Blue Sky Research, USA) coupled with a pinhole aperture in the microscope was used to generate an illumination spot along the fluorescence optical path. A 40× microscope objective was used to precisely focus the excitation light onto the 3D-focused particle/cell stream. To detect the fluorescence emission signal, a dichroic and narrow-bandpass optical filters (480/520 nm) and a photo-multiplier tube (PMT, H6780-20, Hamamatsu, NJ) were attached to the microscope. A digital oscilloscope (DPO400,
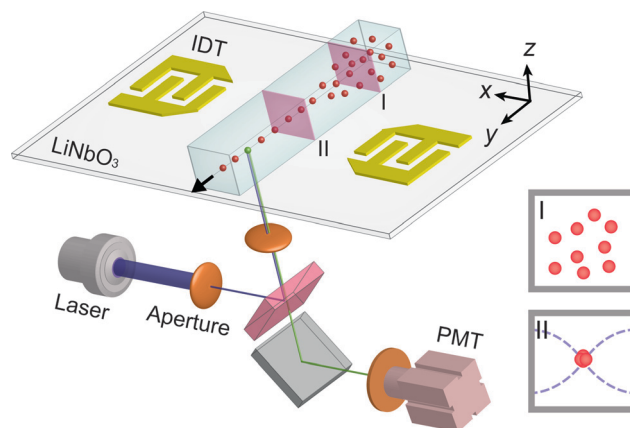

Fig. 1 Schematic of the SSAW-based microfluidic cytometer. A microfluidic device is integrated with a LIF detection system. The insets illustrate cross-sectional views of particle flow patterns before (I) and after (II) SSAW focusing.

Tektronix, USA) was connected to the PMT output to record the electric signal at a sampling rate of 25 kHz. The data collected from the oscilloscope were analyzed with Origin 8.0 and MATLAB software packages.

Sample preparation

Ten micron diameter calibration beads (Flow-Check™ fluorospheres, Beckman Coulter, USA), which had a concentration of 1×10^6 particles mL^{-1}, were used to characterize the microfluidic cytometer. These fluorospheres contained a dye with an excitation wavelength of 488 nm and an emission wavelength from 525 nm to 700 nm. Also, polystyrene fluorescent particles (Dragon Green, Bangs Laboratories, USA) with a diameter of 7.32 μm were diluted to 1.5×10^6 particles mL^{-1} with a 0.1% SDS solution and mixed with the calibration beads in a ratio of 1.5 : 1 for flow cytometry measurements. The samples were sonicated for 5 min before experiments to prevent aggregation. Fluorescently labeled (Calcein AM, BD Biosciences, USA) human promyelocytic leukemia cells (HL-60) with a concentration of $\sim 1 \times 10^5$ cells mL^{-1} were also used to characterize the performance of our SSAW-based microfluidic cytometry.

Results and discussion

SSAW-based 3D focusing

The schematic of the microdevice is shown in Fig. 1. Two parallel IDTs generated a 1D SSAW field with a single pressure node (minimum pressure) covered by the PDMS microchannel. Particles were randomly distributed after they were injected into the microchannel (cross sectional view I). As soon as the particles entered the SSAW field, the lateral primary acoustic radiation force (in the x direction) and the vertical component of the primary force (in z direction) moved the particles from their original paths to the pressure node point located in the center of the microchannel, resulting in 3D focusing of the

microparticles (cross sectional view II). The acoustic radiation force applied on a particle can be expressed as[68,69]

$$F_r = -\left(\frac{\pi p_0{}^2 V_p \beta_m}{2\lambda}\right)\phi(\beta,\rho)\sin\left(\frac{4\pi x}{\lambda}\right) \tag{1}$$

$$\phi = \frac{5\rho_p - 2\rho_m}{2\rho_p + \rho_m} - \frac{\beta_p}{\beta_m} \tag{2}$$

where p_0, V_p, λ, x, ρ_m, ρ_p, β_m, and β_p are the pressure amplitude, the particle volume, the SSAW wavelength, the distance from the pressure node, the density of the medium, the density of particles, the compressibility of the medium, and the compressibility of the particles respectively. The device parameters, including acoustic frequency and power, material properties of the channel, and the channel geometry, can all influence the acoustic energy distribution on the x–z plane. To generate a minimum acoustic energy area or single focal point in the z-direction for effective 3D focusing, it is necessary to synergistically optimize all the parameters.[64] To narrow down the particle focusing width, a relatively strong acoustic radiation force around the focal point will be helpful. As a result, with a relatively high input power, proper acoustic frequency, and optimized channel dimension, one can achieve a fine focal width (in both horizontal and vertical directions) and highly focused particle stream in three dimensions.

We experimentally demonstrated the SSAW-based 3D focusing from both top (as shown in I in Fig. 2A) and side (as shown in II in Fig. 2A) views. The top view (horizontal plane) image was observed directly by a microscope in a bright field, while fluorescent images were observed in the side view (vertical plane) using a prism. Fig. 2B and C show the top-view and side-view images which compare the distribution of particles in a microchannel without (OFF) and with (ON) focusing
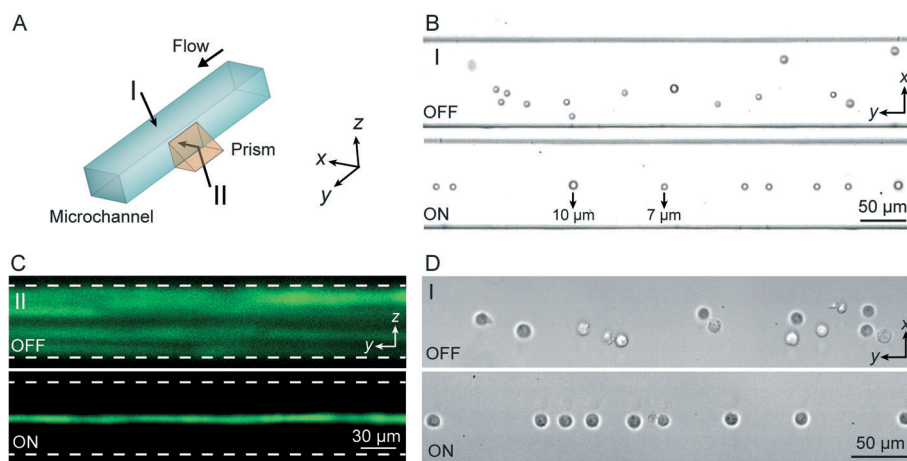

Fig. 2 (A) SSAW-based 3D particle focusing observed from different perspectives (I: top view, II: side view). (B) Top-view bright field images and (C) side-view fluorescent stacking images of the particle flow pattern without (OFF) and with (ON) SSAW focusing. The dashed lines in (C) indicate the channel boundaries. (D) Top-view images showing cell focusing by SSAW. Please refer to ESI† Video 1.

by SSAW. Fig. 2B shows bright-field images recorded from top view (perspective I in Fig. 2A) by a high-speed camera. A mixture of 7 and 10 μm particles were injected into the microchannel at a flow rate of 15 μl min^{-1}. SSAW-based focusing independent of particle size was demonstrated in the bottom image of Fig. 2B, in which both 7 and 10 μm particles were focused into a single-file stream after SSAW was on. Although particles with a smaller size experienced smaller acoustic radiation forces according to eqn (1), they were able to be well focused once the flow rate, the input power, and the length of the SSAW-activated region were optimized to apply sufficient forces on the particles.[70] Fig. 2C shows fluorescent stacking images recorded from side view (perspective II in Fig. 2A) by a CCD camera. Without SSAW focusing (top image of Fig. 2C), particles were travelling on different paths along the entire depth of the microchannel, making it difficult for uniform laser excitation. In the presence of a SSAW field (bottom image of Fig. 2C), the randomly distributed particles were focused into a straight line with identical trajectories, allowing for consistent laser illumination and measurement. In addition to polystyrene microspheres, cells were also able to be focused in the center of the channel (pressure node) by SSAW, as shown in Fig. 2D, which demonstrated that SSAW can be used to effectively focus biological samples.

Device characterization

We used 10 μm fluorospheres as calibration particles to characterize the performance of the microfluidic cytometer. Each particle passed through the illumination spot and emitted a fluorescent signal. The fluorescent signal was detected by a PMT, resulting in the generation of a voltage peak on the oscilloscope. Fig. 3A shows a typical data record of the fluorescent peaks. Only 100 ms of the results are shown in the figure in order to clearly identify each individual peak. In the plot, most of the peak values, which reflect the intensities of the emission signal (photon count), were distributed in a narrow range (3.5 ± 0.3 V). The uniform peak intensities in the data plot indicated a consistent measurement of the calibration particles. This uniformity is usually characterized by calculating the coefficient of variation (CV). The CV is defined as the ratio of the standard deviation to the mean value. Therefore, a smaller CV for the peak intensity indicates a higher-precision flow cytometry measurement, and thus more effective particle focusing. We recorded the fluorescent peaks over a time period of 6 s and a histogram of their intensity (voltage) distribution is shown in Fig. 3B. In this measurement, a total number of 5680 fluorescent peaks were detected, equivalent to a throughput of 946 particles s^{-1}. The peak intensities exhibited a Gaussian distribution with an average intensity of 3.53 V. The CV was calculated to be 9.2%, which is lower when compared to many other reported microfluidic cytometers (>15%).[46,71–75] To further demonstrate the ability of the SSAW-based focusing for flow cytometry, we collected the fluorescent signals without SSAW focusing as a negative control for comparison, which is shown in Fig. 3C. Because the non-focused particles had different trajectories in the microchannel, a large number of them missed the excitation light spot or moved in different planes along the vertical direction, resulting in a much lower number of peaks detected (~110 particles s^{-1}) with a larger non-uniformity in peak intensities (CV = 51.1%) for this control experiment.
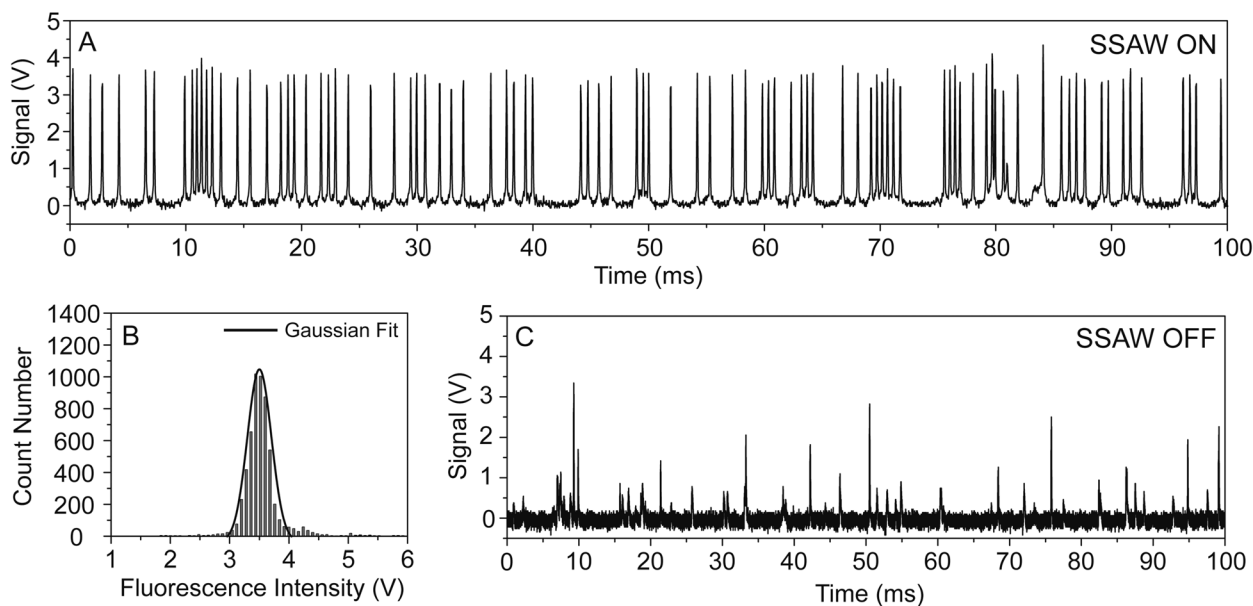

Fig. 3 (A) A typical data trace of fluorescent peaks measured by the LIF detection module of the SSAW-based microfluidic cytometer using 10 μm calibration beads. (B) The distribution of peak intensities recorded over 6 s using SSAW focusing, which exhibited a Gaussian distribution. (C) A data record of fluorescent peaks measured without SSAW focusing shows a much lower particle count and non-uniform distribution.

Flow cytometry measurements of heterogeneous microparticle samples

We used a mixture of 10 μm and 7 μm fluorescent particles as a sample for flow cytometry measurements. A plot of PMT voltages measuring fluorescent emission over a 250 ms time interval is shown in Fig. 4. It is important to note that two distinct levels of peak intensities were observed, corresponding to the different sized particles. The peak profiles recorded between 115 ms and 165 ms are magnified and are re-plotted in the upper inset of Fig. 4. Two groups of fluorescent peaks were clearly identified, revealing that our microfluidic cytometer had the ability to measure particles with different fluorescence emission intensities. We measured the flow of the mixed particles for 4 s and the distribution of the peak intensities is shown in Fig. 5A. To filter out the noise peaks in the emission signals, we set the threshold height at 20% for peak filtering. The total number of fluorescent peaks detected in 4 s was 5235 counts, indicating a throughput of 1309 particles s^{-1}. The histogram shows that the two groups of peak intensities are well separated and fit into two distinct Gaussian distributions. This clearly identifies two different sized particles. The peak intensities for the 7 and 10 μm particles centered at ~1.55 V and ~3.52 V, respectively. Using 2.5 V as the critical value differentiating between the two particle intensities, there were 3087 fluorescent peaks classified as 7 μm particles (<2.5 V), compared to 2148 peaks for 10 μm particles (>2.5 V). This yields a ratio of 1.44 : 1 between the two different particles, which roughly matches the ratio of the two particle concentrations (1.5 : 1). The CV was calculated to be 19.4% for the 7 μm particles and 10.9% for the 10 μm particles. A relatively higher CV for the smaller particles, or at
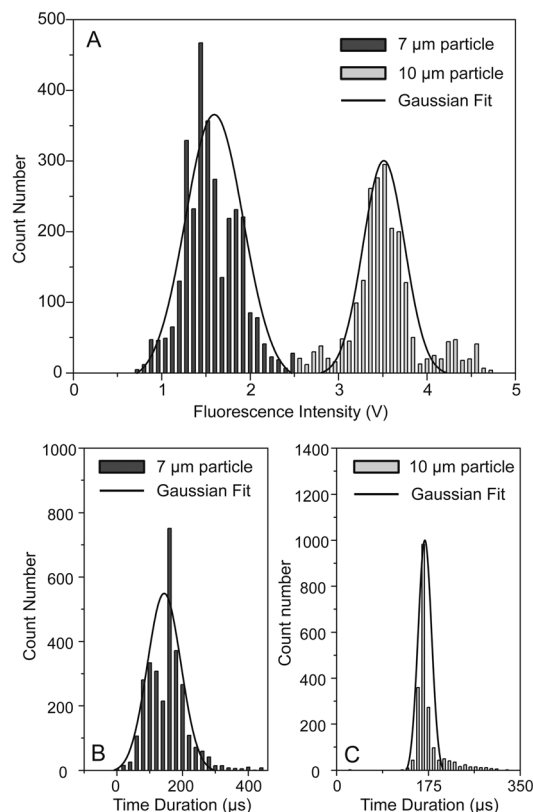

Fig. 5 (A) Distribution of peak intensities used for characterizing SSAW-based cytometry of 7 and 10 μm microparticles. Two Gaussian distributions indicate the two different types of particles. (B) and (C) The distribution of 7 and 10 μm particles based on the time duration through the detection area.

lower fluorescence emission intensities, is common to other flow cytometry techniques as well.[28,31,32,74]
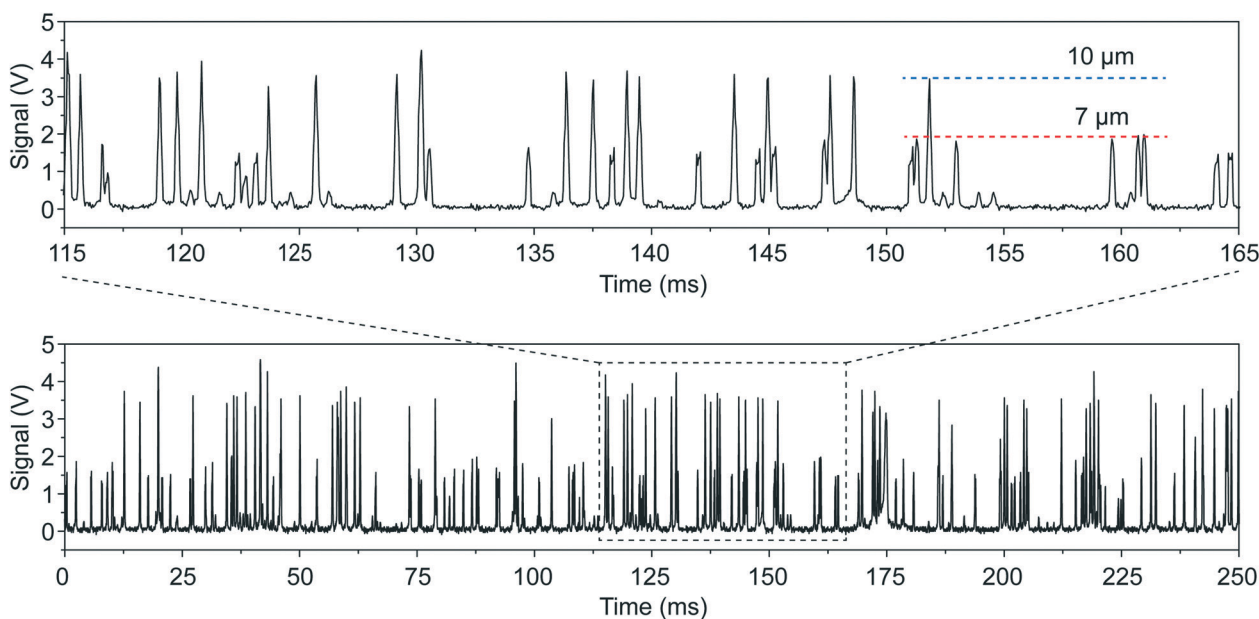

Fig. 4 A data plot of fluorescent peak signals (bottom plot) showing the simultaneous measurement of two types of microparticles with different diameters (7 and 10 μm). The upper inset is an exploded plot focusing on a time interval of only 50 ms where the signal levels from different diameter particles is clearly visible.
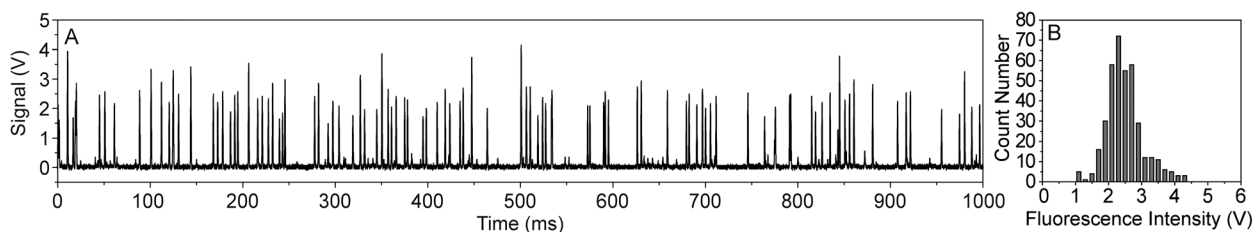
Fig. 6 (A) A data plot of fluorescent peak signals showing the measurement of HL-60 cell with the SSAW-based microfluidic cytometer. (B) The distribution of peak intensities recorded over 4 s using SSAW focusing.

The full width at half maximum (FWHM) of a fluorescent peak represents the characteristic passage time of a particle through a laser illumination spot. We measured the FWHM of all the fluorescent peaks detected during the entire 4 s interval. The distribution of the passage times is shown in Fig. 5B and C for the two different sized particles. The mean passage time was 155 μs for the 7 μm particles and 172 μs for the 10 μm particles, which was in agreement with the particle velocity ($\sim10^5$ μm s^{-1}) and the diameter of the laser illumination spot (~20 μm). The Gaussian distributions of the passage times can be attributed to the 3D focusing effect of the SSAW, without which, the particle velocities would exhibit a much larger variation range due to the flow velocity profile.

Flow cytometer measurements of biological cells

After testing with fluorescent polystyrene microspheres, we then used fluorescently labeled human promyelocytic leukemia cells (HL-60) to further demonstrate the applicability of our SSAW-based flow cytometer to cellular samples. The fluorescence signals collected by the PMT are shown in Fig. 6A. The cell sample had a higher heterogeneity than that of microparticles, resulting in less uniformity of the peak intensities. The distribution of the peak intensities measured in 4 s is shown in Fig. 6B after filtering out the noise signal, with a CV calculated to be 22.0%. The Gaussian distribution of the fluorescent peak intensities with an average value of 2.48 V demonstrated an effective measurement of HL-60 cells with this SSAW-based microfluidic cytometer.

Conclusions

In this work, we demonstrated and characterized a novel SSAW-based microfluidic cytometer, which integrated a SSAW-based 3D focusing technique with a LIF detection system. Experimentally, we successfully performed flow cytometry measurements on calibration beads and measured a CV lower than 10% at a throughput of ~1000 particles s^{-1}. With this SSAW-based microfluidic cytometer, two different groups of particles were clearly identified. Moreover, HL-60 cells could be focused and measured with this system, indicating its applicability to biological samples. Compared to previous works, our system can perform precise flow cytometry with the advantages of sheathless cell focusing, bio-compatibility,

simple and compact device, and significantly reduced biohazards. With further improvements, the SSAW-based microdevice presented here can be developed into a fully integrated, multi-parametric, and portable flow cytometer.

Acknowledgements

References

1 M. Brown and C. Wittwer, *Clin. Chem.*, 2000, **46**, 1221–1229.
2 L. S. Cram, *Methods Cell Sci.*, 2002, **24**, 1–9.
3 M. I. Lapsley, L. Wang and T. J. Huang, *Biomarkers Med.*, 2013, **7**, 75–78.
4 Q. Wei, E. McLeod, H. Qi, Z. Wan, R. Sun and A. Ozcan, *Sci. Rep.*, 2013, **3**, 1699.
5 H. Zhu, S. Mavandadi, A. F. Coskun, O. Yaglidere and A. Ozcan, *Anal. Chem.*, 2011, **83**, 6641–6647.
6 J. Godin, C. H. Chen, S. H. Cho, W. Qiao, F. Tsai and Y. H. Lo, *J. Biophotonics*, 2008, **1**, 355–376.
7 S. H. Cho, J. M. Godin, C. H. Chen, W. Qiao, H. Lee and Y. H. Lo, *Biomicrofluidics*, 2010, **4**, 043001.
8 T. D. Chung and H. C. Kim, *Electrophoresis*, 2007, **28**, 4511–4520.
9 A. Terray and S. J. Hart, *Lab Chip*, 2010, **10**, 1729–1731.
10 N. Watkins, B. M. Venkatesan, M. Toner, W. Rodriguez and R. Bashir, *Lab Chip*, 2009, **9**, 3177–3184.
11 G. Goddard, J. C. Martin, S. W. Graves and G. Kaduchak, *Cytometry, Part A*, 2006, **69**, 66–74.
12 S. Eyal and S. R. Quake, *Electrophoresis*, 2002, **23**, 2653–2657.
13 F. Guo, M. I. Lapsley, A. A. Nawaz, Y. Zhao, S.-C. Lin, Y. Chen, S. Yang, X.-Z. Zhao and T. J. Huang, *Anal. Chem.*, 2012, **84**, 10745–10749.
14 F. Guo, J. B. French, P. Li, H. Zhao, C. Y. Chan, J. R. Fick, S. J. Benkovic and T. J. Huang, *Lab Chip*, 2013, **13**, 3152–3162.
15 C. Zhao, Y. Liu, Y. Zhao, N. Fang and T. J. Huang, *Nat. Commun.*, 2013, **4**, 2305–2313.

16 S. Yang, F. Guo, B. Kiraly, X. Mao, M. Lu and T. J. Huang, *Lab Chip*, 2012, **12**, 2097–2102.

17 G. M. Whitesides, *Nature*, 2006, **442**, 368–373.

18 P. Neuzil, S. Giselbrecht, K. Länge, T. J. Huang and A. Manz, *Nat. Rev. Drug Discovery*, 2012, **11**, 620–632.

19 X. Mao and T. J. Huang, *Lab Chip*, 2012, **12**, 1412–1416.

20 Y. Zhao, Z. S. Stratton, F. Guo, M. I. Lapsley, C. Y. Chan, S.-C. S. Lin and T. J. Huang, *Lab Chip*, 2013, **13**, 17–24.

21 X. Xuan, J. Zhu and C. Church, *Microfluid. Nanofluid.*, 2010, **9**, 1–16.

22 J. Skommer, J. Akagi, K. Takeda, Y. Fujimura, K. Khoshmanesh and D. Wlodkowic, *Biosens. Bioelectron.*, 2013, **42**, 586–591.

23 C. Kunstmann-Olsen, J. D. Hoyland and H.-G. Rubahn, *Microfluid. Nanofluid.*, 2012, **12**, 795–803.

24 J. Wang, B. Fei, R. L. Geahlen and C. Lu, *Lab Chip*, 2010, **10**, 2673–2679.

25 J. Wang, N. Bao, L. L. Paris, R. L. Geahlen and C. Lu, *Anal. Chem.*, 2008, **80**, 9840–9844.

26 C. Simonnet and A. Groisman, *Anal. Chem.*, 2006, **78**, 5653–5663.

27 A. Kummrow, J. Theisen, M. Frankowski, A. Tuchscheerer, H. Yildirim, K. Brattke, M. Schmidt and J. Neukammer, *Lab Chip*, 2009, **9**, 972–981.

28 M. Rosenauer, W. Buchegger, I. Finoulst, P. Verhaert and M. Vellekoop, *Microfluid. Nanofluid.*, 2011, **10**, 761–771.

29 Y.-J. Chiu, S. H. Cho, Z. Mei, V. Lien, T.-F. Wu and Y.-H. Lo, *Lab Chip*, 2013, **13**, 1803–1809.

30 X. Mao, J. R. Waldeisen and T. J. Huang, *Lab Chip*, 2007, **7**, 1260–1262.

31 X. Mao, S.-C. S. Lin, C. Dong and T. J. Huang, *Lab Chip*, 2009, **9**, 1583–1589.

32 X. Mao, A. A. Nawaz, S.-C. S. Lin, M. I. Lapsley, Y. Zhao, J. P. McCoy, W. S. El-Deiry and T. J. Huang, *Biomicrofluidics*, 2012, **6**, 024113.

33 R. Scott, P. Sethu and C. K. Harnett, *Rev. Sci. Instrum.*, 2008, **79**, 046104.

34 C.-C. Fu, G. Ossato, M. Long, M. A. Digman, A. Gopinathan, L. P. Lee, E. Gratton and M. Khine, *Appl. Phys. Lett.*, 2010, **97**, 203101.

35 C. Chang, Z. Huang and R. Yang, *J. Micromech. Microeng.*, 2007, **17**, 1479–1486.

36 C. Simonnet and A. Groisman, *Appl. Phys. Lett.*, 2005, **87**, 114104.

37 N. Sundararajan, M. Pio, L. Lee and A. Berlin, *J. Microelectromech. Syst.*, 2004, **13**, 559–567.

38 P. Howell, J. Golden, L. Hilliard, J. Erickson, D. Mott and F. Ligler, *Lab Chip*, 2008, **8**, 1087–1096.

39 J. Zhou and I. Papautsky, *Lab Chip*, 2013, **13**, 1121–1132.

40 A. Asgar and S. Bhagat, *Biomed. Microdevices*, 2010, **12**, 187–195.

41 M. E. Piyasena, P. P. A. Suthanthiraraj, R. W. Applegate, A. M. Goumas, T. A. Woods, G. P. López and S. W. Graves, *Anal. Chem.*, 2012, **84**, 1831–1839.

42 A. A. S. Bhagat, S. S. Kuntaegowdanahalli, N. Kaval, C. J. Seliskar and I. Papautsky, *Biomed. Microdevices*, 2010, **12**, 187–195.

43 S. C. Hur, H. T. K. Tse and D. D. Carlo, *Lab Chip*, 2010, **10**, 274–280.

44 A. J. Chung, D. R. Gossett and D. D. Carlo, *Small*, 2013, **9**, 685–690.

45 S. Yang, J. Y. Kim, S. J. Lee, S. S. Lee and J. M. Kim, *Lab Chip*, 2011, **11**, 266–273.

46 H. Chu, I. Doh and Y. H. Cho, *Lab Chip*, 2009, **9**, 686–691.

47 L. Wang, L. A. Flanagan, N. L. Jeon, E. Monuki and A. P. Lee, *Lab Chip*, 2007, **7**, 1114–1120.

48 L.-M. Fu, R.-J. Yang, C.-H. Lin, Y.-J. Pan and G.-B. Lee, *Anal. Chim. Acta*, 2004, **507**, 163–169.

49 T.-H. Wang, Y. Peng, C. Zhang, P. K. Wong and C.-M. Ho, *J. Am. Chem. Soc.*, 2005, **127**, 5354–5359.

50 X. Ding, P. Li, S.-C. S. Lin, Z. S. Stratton, N. Nama, F. Guo, D. Slotcavage, X. Mao, J. Shi, F. Costanzo and T. J. Huang, *Lab Chip*, 2013, **13**, 3626–3649.

51 S. Li, X. Ding, F. Guo, Y. Chen, M. Lapsley, S.-C. S. Lin, L. Wang, J. P. McCoy, C. Cameron and T. J. Huang, *Anal. Chem.*, 2013, **85**, 5468–5474.

52 X. Ding, S.-C. S. Lin, B. Kiraly, H. Yue, S. Li, I. K. Chiang, J. Shi, S. J. Benkovic and T. J. Huang, *Proc. Natl. Acad. Sci. U. S. A.*, 2012, **109**, 11105–11109.

53 S.-C. S. Lin, X. Mao and T. J. Huang, *Lab Chip*, 2012, **12**, 2766–2770.

54 R. Wilson, J. Reboud, Y. Bourquin, S. L. Neale, Y. Zhang and J. M. Cooper, *Lab Chip*, 2011, **11**, 323–328.

55 J. Reboud, Y. Bourquin, R. Wilson, G. S. Pall, M. Jiwaji, A. R. Pitt, A. Graham, A. P. Waters and J. M. Cooper, *Proc. Natl. Acad. Sci. U. S. A.*, 2012, **109**, 15162–15167.

56 R. Walker, I. Gralinski, K. Keong Lay, T. Alan and A. Neild, *Appl. Phys. Lett.*, 2012, **101**, 163504.

57 D. J. Collinsa, T. Alana, K. Helmersonb and A. Neild, *Lab Chip*, 2013, **13**, 3225–3231.

58 J. J. Hawkes, R. W. Barber, D. R. Emerson and W. T. Coakley, *Lab Chip*, 2004, **4**, 446–462.

59 J. J. Hawkes, M. J. Long, W. T. Coakley and M. McDonnell, *Biosens. Bioelectron.*, 2004, **19**, 1021–1028.

60 Z. Fan, Y. Sun, D. Chen, D. Tay, W. Chen, C. X. Deng and J. Fu, *Sci. Rep.*, 2013, **3**, 2176.

61 X. Ding, S.-C. S. Lin, M. I. Lapsley, S. Li, X. Guo, C. Y. Chan, I.-K. Chiang, J. P. McCoy and T. J. Huang, *Lab Chip*, 2012, **12**, 4228–4231.

62 X. Ding, J. Shi, S.-C. S. Lin, S. Yazdi, B. Kiraly and T. J. Huang, *Lab Chip*, 2012, **12**, 2491–2497.

63 J. Shi, X. Mao, D. Ahmed, A. Colletti and T. J. Huang, *Lab Chip*, 2008, **8**, 221–223.

64 J. Shi, S. Yazdi, S.-C. S. Lin, X. Ding, I.-K. Chiang, K. Sharp and T. J. Huang, *Lab Chip*, 2011, **11**, 2319–2324.

65 J. Shi, D. Ahmed, X. Mao, S.-C. S. Lin, A. Lawit and T. J. Huang, *Lab Chip*, 2009, **9**, 2890–2895.

66 Y. Chen, X. Ding, S.-C. S. Lin, S. Yang, P.-H. Huang, N. Nama, Y. Zhao, A. A. Nawaz, F. Guo and W. Wang, *et al.*, *ACS Nano*, 2013, **7**, 3306–3314.

67 Q. Zeng, F. Guo, L. Yao, H. W. Zhu, L. Zheng, Z. X. Guo, W. Liu, Y. Chen, S. S. Guo and X. Z. Zhao, *Sens. Actuators, B*, 2011, **160**, 1552–1556.

68 K. Yosioka and Y. Kawasima, *Acustica*, 1955, **5**, 167–173.

69 A. Nilsson, F. Petersson, H. Jonsson and T. Laurell, *Lab Chip*, 2004, **4**, 131–135.

70 J. Shi, H. Huang, Z. Stratton, Y. Huang and T. J. Huang, *Lab Chip*, 2009, **9**, 3354–3359.

71 Z. Wang, J. El-Ali, M. Engelund, T. Gotsæd, I. R. Perch-Nielsen, K. B. Mogensen, D. Snakenborg, J. P. Kutter and A. Wolff, *Lab Chip*, 2004, **4**, 372–377.

72 D. P. Schrum, C. T. Culbertson, S. C. Jacobson and J. M. Ramsey, *Anal. Chem.*, 1999, **71**, 4173–4177.

73 M. A. McClain, C. T. Culbertson, S. C. Jacobson and J. M. Ramsey, *Anal. Chem.*, 2001, **73**, 5334–5338.

74 S.-C. Lin, P.-W. Yen, C.-C. Peng and Y.-C. Tung, *Lab Chip*, 2012, **12**, 3135–3141.

75 N. Pamme, R. Koyama and A. Manz, *Lab Chip*, 2003, **3**, 187–192.